Biol. Cybern. 81, 415–424 (1999)

Biological Cybernetics

Nonlinear EEG analysis based on a neural mass model

P.A. Valdes[1], **J.C. Jimenez**[1], **J. Riera**[1], **R. Biscay**[1], **T. Ozaki**[2]

[1] Cuban Neuroscience Center (CNIC), P.O.Box 6880, Havana, Cuba
[2] The Institute of Statistical Mathematics, Tokyo, Japan

Received: 11 August 1997 / Accepted in revised form: 20 April 1999

Abstract. The well-known neural mass model described by Lopes da Silva et al. (1976) and Zetterberg et al. (1978) is fitted to actual EEG data. This is achieved by reformulating the original set of integral equations as a continuous-discrete state space model. The local linearization approach is then used to discretize the state equation and to construct a nonlinear Kalman filter. On this basis, a maximum likelihood procedure is used for estimating the model parameters for several EEG recordings. The analysis of the noise-free differential equations of the estimated models suggests that there are two different types of alpha rhythms: those with a point attractor and others with a limit cycle attractor. These attractors are also found by means of a nonlinear time series analysis of the EEG recordings. We conclude that the Hopf bifurcation described by Zetterberg et al. (1978) is present in actual brain dynamics.

1 Introduction

It has been recognized for some years (Wiener 1958) that the electroencephalogram (EEG) reflects the activity of a complex nonlinear dynamic system comprising a very large number of neurons (Lopes da Silva 1993). The role of nonlinearity in the EEG is supported by recent studies using statistical nonlinear time series analysis (Ozaki 1985; Priestley 1988; Tong 1990)[1]. Indeed, Hernandez et al. (1995a, b, 1996) have shown that nonlinear time series models such as kernel nonlinear autoregression (Auestad and Tjøstheim 1990) are able to describe limit cycle behavior in EEG recordings of alpha rhythm, different types of slow wave activities and spike and waves.

Correspondence to: P. Valdes Sosa
(e-mail: peter@cneuro.edu.cu, Fax: +53-7-336321)

[1] See J R Stat Soc Ser B (1992) 54 (2): 301–474, dedicated to chaos and time series analysis.

A number of authors have attempted to model the EEG at a macroscopic level by means of sets of differential equations or integral-differential equations. Wilson and Cowan (1972) showed that a set of two first-order differential equations exhibits limit cycle behavior and hysteresis phenomena. They suggested that the rhythmic activity generated by this model mimic the EEG, a conclusion supported subsequently by Freeman (1975). Lopes da Silva et al. (1974) showed that noise passed through a nonlinear filter produces activity similar to the alpha rhythm. In fact, this model was capable of predicting changes in the spectrum with maturation that have been documented statistically (compare the figure of Lopes da Silva et al. 1974, with that presented in Szava et al. 1994). Further work with this type of model suggested that phenomena such as epileptic spikes and seizures could reflect instability of the dynamic system (Lopes da Silva et al. 1976; Kaczmarek and Babloyantz 1977; Zetterberg et al. 1978). This line of work is being notably developed by the construction of the structural portrait of these models (Borisyuk and Kirilov 1992).

What has been lacking is a direct link between empirical descriptions of the EEG as a nonlinear time series and the theoretical predictions of neural mass models. Consequently, there is little work in fitting and validating theoretical models for actual EEG data. A basic obstacle seems to be the general difficulty of translating the continuous equations of the neural mass models into discrete time series models. Recently, a "bridge" between nonlinear stochastic dynamic systems and nonlinear time series models has been developed based on the "local linearization" (LL) approach (Ozaki 1985, 1992, 1993, 1994). This method allows construction of a stable discretization of nonlinear stochastic differential equations and an adequate identification of state space models from observed time series.

This paper focuses on the statistical fitting of the neural mass model described by Lopes da Silva et al. (1976) and Zetterberg et al. (1978) to EEG data. This is achieved by reformulating the original set of integral equations as a continuous-discrete state space model.

Thus, the LL approach is used to discretize the state equation and to construct a nonlinear Kalman filter. On this basis, a maximum likelihood procedure is used for estimating the model parameters for several EEG recordings. Then, the qualitative behavior of the noise-free differential equation of estimated models and the noise-free realization of a nonlinear time series model fitted to each EEG recording are compared.

The paper is organized as follows: the original neural mass model is summarized in Sect. 2. Section 3 presents the model in state space form. Section 4 summarizes the LL technique for discretization and identification of models. Section 5 presents examples of the use of the LL method in simulation, fitting and analysis of the alpha rhythm. Finally, Sect. 6 discusses the results and points out areas that need further development.

2 Neural mass model

A general class of neural mass models was described earlier by Freeman (1975) in terms of a hierarchical classification of interacting sets of neurons. In his terminology, a KIe (KIi) set is a conglomerate of interconnected excitatory (inhibitory) neurons with a common input and output. The neural mass model under discussion in this paper is an example of a model introduced by Zetterberg et al. (1978), which in turn belongs to the more general class of Freeman's models. It comprises two KIe excitatory neural sets (KIe1 and KIe2) interconnected with a KIi inhibitory neural set [see Fig. 1, which is derived from Fig. 1b in Zetterberg et al. (1978) by setting $C_5 = 0$ and $P_1(t) = 0$].

The model is formulated in terms of the following variables: the proportion of cells firing per unit of time at time t in each population ($E_1(t)$, $E_2(t)$ and $I(t)$ in KIe1, KIe2 and KIi, respectively) and the average membrane potentials of each population ($V_{1e}(t)$, $V_{2e}(t)$ and $V_i(t)$ in KIe1, KIe2 and KIi, respectively). The former are related to the latter by the sigmoid shape function g as initially described by Freeman (1975) and modified by Zetterberg et al. (1978). These relations are formally expressed by

$$E_1(t) = g[V_{1e}(t)] \ , \tag{1}$$

$$E_2(t) = g[V_{2e}(t)] \ , \tag{2}$$

$$I(t) = g[V_i(t)] \ , \tag{3}$$

where:

$$g(V) = \begin{cases} g_0\lambda e^{\gamma(V-V_0)} & V \le V_0 \\ g_0\lambda\left[2 - e^{-\gamma(V-V_0)}\right] & V > V_0 \ . \end{cases} \tag{4}$$

For the specification of the constants $g_0\lambda$, γ and V_0 (see Table 1).

The action potentials spreading through axons are transformed into post-synaptic potentials (PSP) in synaptic terminals. The latter propagating through the dendrites reach other cells with a certain delay and attenuation, then they are linearly summed to form the average membrane potentials. This is expressed by the equations:

$$V_{1e}(t) = \int_0^\infty (c_4 E_2(t-\tau) + P(t-\tau))h_e(\tau)d\tau - \int_0^\infty c_2 I(t-\tau)h_i(\tau)d\tau \ , \tag{5}$$

$$V_{2e}(t) = \int_0^\infty c_3 E_1(t-\tau)h_e(\tau)d\tau \ , \tag{6}$$

$$V_i(t) = \int_0^\infty c_1 E_1(t-\tau)h_e(\tau)d\tau \ , \tag{7}$$

where the parameters c_1, c_2, c_3 and c_4 denote the synaptic efficiency with which each neural set influences the others. Here, the impulse functions $h_r(\tau) = A_r\lfloor e^{-a_r\tau} - e^{-b_r\tau}\rfloor$, $r = \{e, i\}$, depend on constants defined in Table 1. The external input to the whole system is represented by $P(t)$ which is assumed to be a Gaussian white noise with mean Π and variance σ_P^2.

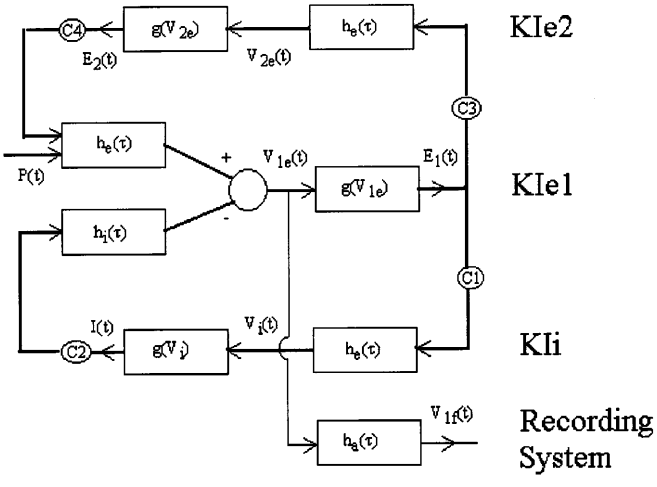

Fig. 1. Block diagram of the neuronal populations involved in the mass model, which comprises two excitatory neural sets (*KIe*1 and *KIe*2) interconnected with an inhibitory neural set (*KIi*). The recording system is also displayed

Table 1. Constants involved in the definition of the neural model

Symbol	Definition	Units	Value
$g_0\lambda$	Maximum value of the function g	s^{-1}	25
γ	Scale parameter of the function g	MV^{-1}	0.34
V_o	Voltage offset of the function g	MV	6
A_e	Maximum of h_e	MV	1.6
a_e	Time constant of h_e	s^{-1}	55
b_e	Time constant of h_e	s^{-1}	605
A_i	Maximum of h_i	MV	32
a_i	Time constant of h_i	s^{-1}	27.5
b_i	Time constant of h_i	s^{-1}	55
τ	Time constant of the high pass filter h_a	s	0.32
δ	Damping factor of the filter h_a	s	0.707
ω_n	Angular high cut frequency of the filter of h_a	Hz	2π 30

In this paper, time delays for transmission of activity between different neural sets are ignored. Such delays would transform the system into an infinite-dimensional dynamic system (Gumowski 1981), a complication to be avoided at this step, but certainly an aspect of great physiological importance.

The model just presented includes as a special case the model of Lopes da Silva et al. (1974). Moreover, it exhibits a wide variety of electrical activities: from alpha-like rhythms to recordings with spike-like wave forms (Figs. 5–7 of Zetterberg et al. 1978). Only stationary regimes of the system will be studied in this paper but the analysis of transient behavior is also possible within the general framework developed here.

3 State space formulation of the neural mass model

In order to fit of the neural mass model to the actual EEG data, the neural model is reformulated as a continuous-discrete state space model.

Using the change of variable $u = t - \tau$, the system of Eqs. (5)–(7) can be rewritten as

$$V_{1e}(t) = \int_{-\infty}^{t} [c_4 E_2(u) + P(u)] h_e(t-u)du - \int_{-\infty}^{t} c_2 I(u) h_i(t-u)du \ ,$$

$$V_{2e}(t) = \int_{-\infty}^{t} c_3 E_1(u) h_e(t-u)du \ ,$$

$$V_i(t) = \int_{-\infty}^{t} c_1 E_1(u) h_e(t-u)du \ .$$

Since

$$\lim_{t\to\infty} \int_{-\infty}^{0} f(u) h_e(t-u)du \to 0$$

for any bounded function f, then the solution of the above system of equations is asymptotically equivalent to the solution of

$$V_{1e}(t) = \int_{0}^{t} [c_4 E_2(u) + P(u)] h_e(t-u)du - \int_{0}^{t} c_2 I(u) h_i(t-u)du \ ,$$

$$V_{2e}(t) = \int_{0}^{t} c_3 E_1(u) h_e(t-u)du \ ,$$

$$V_i(t) = \int_{0}^{t} c_1 E_1(u) h_e(t-u)du \ ,$$

when $t \to \infty$.

Thus, applying the Laplace transformation to this system of equations it follows that:

$$V_{1e}(s) = [c_4 E_2(s) + P(s)] H_e(s) - c_2 I(s) H_i(s) \ , \tag{8}$$

$$V_{2e}(s) = c_3 E_1(s) H_e(s) \ , \tag{9}$$

$$V_i(s) = c_1 E_1(s) H_e(s) \ , \tag{10}$$

where

$$H_r(s) = \frac{(b_r - a_r) A_r}{(s + a_r)(s + b_r)}$$

is the Laplace transformation of h_r.

$H_r(s)$ can be rewritten as:

$$H_r(s) = \frac{\varepsilon_r}{L_r(s)} \ ,$$

where $L_r(s) = s^2 - \alpha_r s - \beta_r$, $\varepsilon_r = (b_r - a_r) A_r$, $\alpha_r = -(a_r + b_r)$ and $\beta_r = -a_r b_r$.

Multiplying Eqs. (8)–(10) by $L_r(s)$, they can be rewritten as

$$L_e(s) V_{1e}(s) = \varepsilon_e [c_4 E_2(s) + P(s)] - c_2 L_e(s) I_f(s) \ , \tag{11}$$

$$L_e(s) V_{2e}(s) = \varepsilon_e c_3 E_1(s) \ , \tag{12}$$

$$L_e(s) V_i(s) = \varepsilon_e c_1 E_1(s) \ , \tag{13}$$

where

$$L_i(s) I_f(s) = \varepsilon_i I(s) \ . \tag{14}$$

Applying the inverse Laplace transformation to Eqs. (11)–(14):

$$\ddot{V}_{1e}(t) = \alpha_e \dot{V}_{1e}(t) + \beta_e V_{1e}(t) + \varepsilon_e [c_4 E_2(t) + P(t)] - c_2 \left[\ddot{I}_f(t) - \alpha_e \dot{I}_f(t) - \beta_e I_f(t)\right] \ ,$$

$$\ddot{V}_{2e}(t) = \alpha_e \dot{V}_{2e}(t) + \beta_e V_{2e}(t) + \varepsilon_e c_3 E_1(t) \ ,$$

$$\ddot{V}_i(t) = \alpha_e \dot{V}_i(t) + \beta_e V_i(t) + \varepsilon_e c_1 E_1(t) \ ,$$

$$\ddot{I}_f(t) = \alpha_i \dot{I}_f(t) + \beta_i I_f(t) + \varepsilon_i I(t)$$

Substituting the relations (1)–(3) in the above equation it follows that

$$\ddot{V}_{1e}(t) = \alpha_e \dot{V}_{1e}(t) + \beta_e V_{1e}(t) + \varepsilon_e c_4 g[V_{2e}(t)] - c_2 \left\{-\alpha \dot{I}_f(t) - \beta I_f(t) - \varepsilon_i g[V_i(t)]\right\} + \varepsilon_e P(t) \ , \tag{15}$$

$$\ddot{V}_{2e}(t) = \alpha_e \dot{V}_{2e}(t) + \beta_e V_{2e}(t) + \varepsilon_e c_3 g[V_{1e}(t)] \ , \tag{16}$$

$$\ddot{V}_i(t) = \alpha_e \dot{V}_i(t) + \beta_e V_i(t) + \varepsilon_e c_1 g[V_{1e}(t)] \ , \tag{17}$$

$$\ddot{I}_f(t) = \alpha_i \dot{I}_f(t) + \beta_i I_f(t) + \varepsilon_i g[V_i(t)] \ , \tag{18}$$

where $\alpha = \alpha_e - \alpha_i$ and $\beta = \beta_e - \beta_i$.

In this model, such as it was originally introduced by Zetterberg et al. (1978), the variable that resembled EEG background activity is V_{1e}. Hence, this is taken as the output of the system. However, this variable does not yet take into account the effect of the amplifiers that are used to record the EEG nor the distortions produced by the different tissue layers between the neural mass and the recording electrode.

The effect of the amplifiers of an EEG recording system is filtering of the signal. For the purpose of this paper, a Butterworth filter formed by a cascade of a (second-order) low pass filter and a (first-order) high pass filter will be considered. These are the filters of the recording system "Medicid-04" (see Fundora et al. 1997), which was used to record the data analyzed in Sect. 5. In addition, it has been shown (Hernández et al. 1995c) that the intermediate tissues attenuate the EEG signal with a subject-dependent gain factor. In our model, the gain factor a is incorporated into the amplifier transfer function h_a.

Thus, the observed signal V_{1f} is the result of band-pass filtering of V_{1e} (see Fig. 1), that is

$$V_{1f}(t) = \int_0^\infty V_{1e}(t-\tau) h_a(\tau) d\tau \ ,$$

where the function h_a has the Laplace transform:

$$h_a(s) = \frac{a\tau s}{\tau s + 1} \cdot \frac{\omega_n^2}{s^2 + 2\delta\omega_n s + \omega_n^2} \ .$$

The constants involved in this expression are specified in Table 1.

As is well known, filters with rational transfer functions are characterized by linear ordinary differential equations. Specifically for V_{1f}, the third-order equation is obtained:

$$\frac{d^3 V_{1f}}{dt^3} = \kappa_2 \frac{d^2 V_{1f}}{dt^2} + \kappa_1 \frac{dV_{1f}}{dt} + \kappa_0 V_{1f} + a\omega_n^2 \frac{dV_{1e}}{dt} \ . \qquad (19)$$

where $\kappa_0 = \frac{-\omega_n^2}{\tau}$, $\kappa_1 = \frac{-2\delta\omega_n}{\tau} - \omega_n^2$ and $\kappa_2 = -2\delta\omega_n - \frac{1}{\tau}$.

By introducing new variables, the high order system of differential Eqs. (15)–(19) can be transformed into the first-order system of differential equations:

$$\dot{V}_{1e}^1(t) = \alpha_e V_{1e}^1(t) + \beta_e V_{1e}(t) + \varepsilon_e c_4 g[V_{2e}(t)] + c_2 \alpha I_f^1(t) + c_2 \beta I_f(t) + c_2 \varepsilon_i g[V_i(t)] + \varepsilon_e \Pi + \omega(t) \ ,$$

$$\dot{V}_{2e}^1(t) = \alpha_e V_{2e}^1(t) + \beta_e V_{2e}(t) + \varepsilon_e c_3 g[V_{1e}(t)] \ ,$$

$$\dot{V}_i^1(t) = \alpha_e V_i^1(t) + \beta_e V_i(t) + \varepsilon_e c_1 g[V_{1e}(t)] \ ,$$

$$\dot{I}_f^1(t) = \alpha_i I_f^1(t) + \beta_i I_f(t) + \varepsilon_i g[V_i(t)] \ ,$$

$$\dot{V}_{1e}(t) = V_{1e}^1(t) \ ,$$

$$\dot{V}_{2e}(t) = V_{2e}^1(t) \ ,$$

$$\dot{V}_i(t) = V_i^1(t) \ ,$$

$$\dot{I}_f(t) = I_f^1(t) \ ,$$

$$\dot{V}_{1f}^2 = \kappa_2 V_{1f}^2 + \kappa_1 V_{1f}^1 + \kappa_0 V_{1f} + a\omega_n^2 V_{1e}^1 \ ,$$

$$\dot{V}_{1f}(t) = V_{1f}^1(t) \ ,$$

$$\dot{V}_{1f}^1(t) = V_{1f}^2(t) \ .$$

where ω is a white noise process with zero mean and variance $\varepsilon_e^2 \sigma_P^2$.

This can be expressed most succinctly as the following stochastic differential equation (SDE):

$$\dot{\mathbf{x}} = \mathbf{f}(\mathbf{x}, \boldsymbol{\theta}) + \mathbf{w} \ , \qquad (20)$$

where

$$\mathbf{x} = \left(V_{1e}^1, V_{2e}^1, V_i^1, I_f^1, V_{1e}, V_{2e}, V_i, I_f, V_{1f}^2, V_{1f}, V_{1f}^1\right)^T$$

is the state vector,

$$\mathbf{w} = (\omega, 0, 0, 0, 0, 0, 0, 0, 0, 0, 0)^T$$

is a random vector with zero mean and a 11×11 covariance matrix of the form:

$$\boldsymbol{\Sigma} = \begin{bmatrix} \boldsymbol{\varepsilon}_e^2 \boldsymbol{\sigma}_P^2 & \mathbf{0} \\ \mathbf{0} & \mathbf{0} \end{bmatrix},$$

and $\boldsymbol{\theta} = [c_1 \ c_2 \ c_3 \ c_4 \ \Pi \ \sigma_P^2 \ a]$ is the set of state parameters.

In practice, only the state variable V_{1f} of Eq. (20), contaminated with measurement noise, is observed at the discrete times t_n. This may be modeled as:

$$\mathbf{z}_{t_n} = \mathbf{C}\mathbf{x}_{t_n} + \boldsymbol{\varepsilon}_{t_n} \ , \qquad (21)$$

with $\mathbf{C} = (0, 0, 0, 0, 0, 0, 0, 0, 0, 0, 1, 0)$. The measurement noise $\boldsymbol{\varepsilon}$ is assumed to be a random Gaussian process with zero mean and variance $\boldsymbol{\Sigma}^{\boldsymbol{\varepsilon}\boldsymbol{\varepsilon}}$.

Thus, finally, the state space form for the neural mass model is given by the state Eq. (20) and the observation Eq. (21).

4 LL method

Ozaki (1985, 1993, 1994) has introduced the technique of LL for the integration of SDEs such as Eq. (20) as well as for nonlinear filtering problems and model identification from observed time series. This section summarizes the more recent advances of this technique (Biscay et al. 1996; Jimenez 1996; Ozaki et al. 1996) which will be used in this paper.

Consider the discrete times $t_n = t_0 + n\Delta t$ (for $n = 0, 1, 2, \ldots, N$ and $\Delta t > 0$). Assuming that the system is approximately linear on each interval $[t_n, t_{n+1}]$, the LL discretization of Eq. (20) results in the following non-linear auto-regressive model:

$$\mathbf{x}_{t_{n+1}} = \mathbf{x}_{t_n} + \mathbf{R}[\mathbf{J}(\mathbf{x}_{t_n}), \Delta t]\mathbf{f}(\mathbf{x}_{t_n}, \boldsymbol{\theta}) + \mathbf{n}_{t_n}(\mathbf{x}_{t_n}) \ , \tag{22}$$

where $\mathbf{R}[\mathbf{J}(\mathbf{x}_{t_n}), \Delta t]$ is the matrix function:

$$\mathbf{R}[\mathbf{J}(\mathbf{x}_{t_n}), \Delta t] = \int_0^{\Delta t} \mathrm{e}^{\mathbf{J}(\mathbf{x}_{t_n})s} ds \tag{23}$$

and $\mathbf{n}_{t_{n+1}}$ is a white noise process with zero mean and covariance matrix:

$$\mathbf{Q}_{t_{n+1}}(\mathbf{x}_{t_n}) = \int_0^{\Delta t} \mathrm{e}^{\mathbf{J}(\mathbf{x}_{\mathbf{t_n}})\mathbf{s}} \boldsymbol{\Sigma} \mathrm{e}^{\mathbf{J}^T(\mathbf{x}_{t_n})s} ds \ . \tag{24}$$

Here, $\mathbf{J}$ denotes the Jacobian matrix of $\mathbf{f}$ and $\mathbf{J}^T$ denotes the transpose of $\mathbf{J}$. For details of the computation of expressions (23) and (24), see Biscay et al. (1996) and Jimenez et al. (1998), respectively.

The reconstruction of the complete trajectory $\mathbf{x}_{t_n}$ of the state space model (20)–(21), given the observed time series $\mathbf{z}_{t_n}$, is realized by means of the following nonlinear Kalman filtering algorithm:

$$\mathbf{x}_{t_{n+1}|t_n} = \mathbf{x}_{t_n|t_n} + \mathbf{R}\big[\mathbf{J}(\mathbf{x}_{t_n|t_n}), \Delta t\big]\mathbf{f}(\mathbf{x}_{t_n|t_n}) \ , \tag{25}$$

$$\mathbf{P}_{t_{n+1}|t_n} = \mathrm{e}^{\mathbf{J}(\mathbf{x}_{t_{n+1}|t_n})\Delta t} \mathbf{V}_{t_n} \mathrm{e}^{\mathbf{J}^T(\mathbf{x}_{t_{n+1}|t_n})\Delta t} + \mathbf{Q}_{t_{n+1}}(\mathbf{x}_{t_n|t_n}),$$

$$\upsilon_{t_{n+1}} = \mathbf{z}_{t_{n+1}} - \mathbf{C}\mathbf{x}_{t_{n+1}|t_n} \ , \tag{26}$$

$$\boldsymbol{\Sigma}^{vv}_{t_{n+1}} = \mathbf{C}\mathbf{P}_{t_{n+1}|t_{n+1}}\mathbf{C}^T + \boldsymbol{\Sigma}^{\boldsymbol{\varepsilon\varepsilon}} \ , \tag{27}$$

$$\mathbf{K}_{t_{n+1}} = \mathbf{P}_{t_{n+1}|t_n}\mathbf{C}^T\left(\Sigma^{vv}_{t_{n+1}}\right)^{-1} \ , \tag{28}$$

$$\mathbf{x}_{t_{n+1}|t_{n+1}} = \mathbf{x}_{t_{n+1}|t_n} + \mathbf{K}_{t_{n+1}}\upsilon_{t_{n+1}} \ , \tag{29}$$

$$\mathbf{V}_{t_n} = \mathbf{P}_{t_{n+1}|t_n} - \mathbf{K}_{t_{n+1}}\mathbf{C}\mathbf{P}_{t_{n+1}|t_n} \ , \tag{30}$$

where the vector $\mathbf{x}_{0|0}$ and the matrix $\mathbf{V}_0$ are assumed to be given. This algorithm calculates the filtered values $\mathbf{x}_{t_{n+1}|t_{n+1}}$ of the state variable $\mathbf{x}$ and the innovation function $\upsilon_{t_{n+1}}$ at the N time instants $t_n (n = 0, 1, 2, \ldots, N)$ where the actual EEG signal $\mathbf{z}$ has been observed. This nonlinear filtering technique is the basis for a maximum likelihood procedure that fits the model to data.

The maximum likelihood (ML) estimators of the unknown parameters $\boldsymbol{\theta}$ and $\mathbf{x}_{0|0}$ are obtained by minimizing the negative log likelihood

$$-\ln l\big(\mathbf{z}; \boldsymbol{\theta}; \mathbf{x}_{0|0}\big) = -\ln(2\pi)N + \sum_{k=1}^{N}\left[\ln|\boldsymbol{\Sigma}^{vv}_{t_k}| + \upsilon^T_{t_k}(\boldsymbol{\Sigma}^{vv}_{t_k})^{-1}\upsilon_{t_k}\right] \ , \tag{31}$$

according to the following steps:

1. Selecting some initial values for the parameters $\boldsymbol{\theta}$ and $\mathbf{x}_{0|0}$. The initial value of $\boldsymbol{\theta}$ is chosen from the set of possible values reported by Zetterberg et al. (1978). The initial value of the nonobserved variables of $\mathbf{x}_{0|0}$ is chosen according to Eq. (20), with the initial value of $\boldsymbol{\theta}$ being numerically integrated in a large time interval [0, T] starting with $\mathbf{x}_{t_0} = 0$. After that, $\mathbf{x}_{0|0}$ is set equal to $\mathbf{x}_T$.

2. Selecting an instant of time t_m after which the initial transients in the innovation function $\upsilon^0_{t_{n+1}}$ disappear. The innovation function $\upsilon^0_{t_{n+1}}$ is that obtained from the nonlinear Kalman filtering algorithm [Eqs. (25)–(30)] with the initial values of $\boldsymbol{\theta}$ and $\mathbf{x}_{0|0}$.

3. Minimizing the expression

$$-\ln l\big(\mathbf{z}; \boldsymbol{\theta}; \mathbf{x}_{0|0}\big) = -\ln(2\pi)N + \sum_{k=m}^{N}\left[\ln|\boldsymbol{\Sigma}^{vv}_{t_k}| + \upsilon^T_{t_k}(\boldsymbol{\Sigma}^{vv}_{t_k})^{-1}\upsilon_{t_k}\right] \ ,$$

with respect to the parameter $\boldsymbol{\theta}$ by a numerical optimization procedure.

4. Minimizing Eq. (31) with respect to the parameter $\mathbf{x}_{0|0}$ by a numerical optimization procedure.

The variance $\mathbf{V}_0$ of $\mathbf{x}_{0|0}$ is, in general, a constant diagonal matrix with numbers in the range 10^{-3}–10^{-9}. These are selected by trial and error in such a way as to guarantee a large transient in the innovation function $\upsilon_{t_{n+1}}$ in step 2 above. In this work, $\mathbf{V}_0$ was set to $10^{-6}\mathbf{I}$. The minimization of functions in steps 3 and 4 is carried out under the constraint that the mean and variance of the innovation $\upsilon_{t_{n+1}}$ are smaller than the mean and variance of $\upsilon^0_{t_{n+1}}$.

5 Results

5.1 Simulations of EEG recordings

The numerical integration scheme for SDE, the nonlinear Kalman filter, and the ML estimation procedure discussed above were implemented in Matlab. The results of testing this implementation of the LL method with well-known "benchmark" nonlinear oscillators has been reported elsewhere (Biscay et al. 1996; Jimenez 1996; Ozaki et al. 1996). Additional Matlab modules were coded for the nonlinear state function of the neural mass model.

Realizations of the trajectories of the SDE (Eq. 20) for different sets of state parameters were obtained by numerical integration. The state parameters covered the complete parameter range suggested by Zetterberg et al. (1978). Figures 2 (top left) and 3 (right) show examples of the time evolution of the observed variable V_{1f} for different parameter values. These "simulated EEG" tracings are quite similar in appearance and spectral content to actual EEG recordings (see, e.g., Fig. 2, top right). They are also similar to the recordings presented by Zetterberg et al. (1978), which were obtained by means of an analog electronic device. In fact, it was possible to reconstruct all the figures in Zetterberg et al. (1978), except for Fig. 6a of that paper. In addition, Fig. 2 shows examples of the time evolution of the nonobserved variable V_{1e} (middle left) and V_{2e} (bottom left) and their corresponding spectra.

The LL filter also allows a successful reconstruction of the nonobservable state variables given only obser-

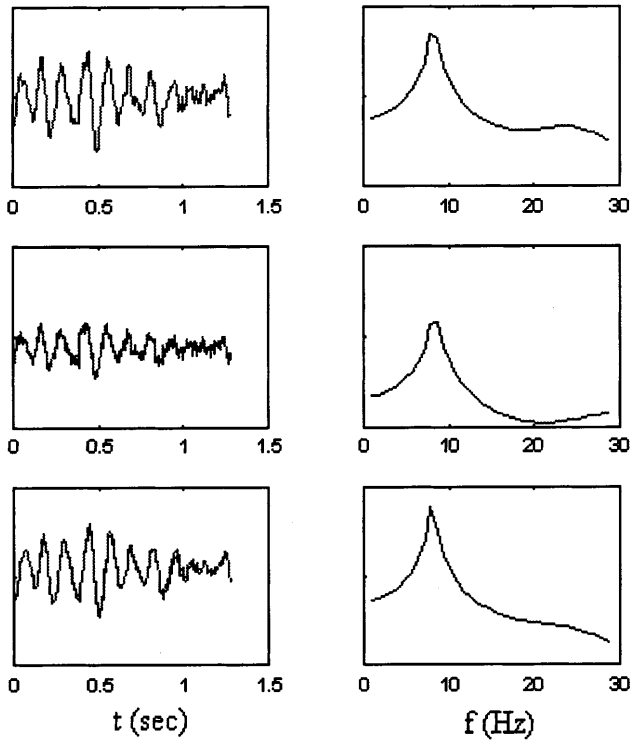

Fig. 2. *Left* Three state variables for one simulation of the alpha rhythm obtained by integration of the neural mass model (*top* V_{1f}, *middle* V_{1e}, and *bottom* V_{2e}). Superimposed on each simulated state variable trajectory is that estimated by the local linearization filter from the observed values of V_{1f}. *Right* Frequency spectra of each state variable

vations of V_{1f}. This is illustrated in Fig. 2 (middle and bottom left) which superimposes the trajectories of the state space variables estimated by filtering upon the true trajectories.

5.2 Nonlinear behavior of actual EEG alpha recordings

A set of nine 1.28-s EEG recordings with alpha rhythm was selected at random from the normative database at the Cuban Neuroscience Center. These recordings, from the derivation O1, were obtained using the Medicid-04 system with a sampling rate of 2000 Hz and a band pass filter of 0.05–30 Hz.

Empirical estimates of the deterministic attractor of each EEG recording were estimated as described in Hernandez et al. (1995a,b, 1996). Nonparametric kernel auto-regressive estimates of the nonlinear state function were applied repeatedly to randomly chosen initial values to produce empirical noise-free realizations (E-NFR) typical of each recording. These, in turn, were used to determine the nonstochastic attractors of the system. The dynamics of E-NFR of alpha-rhythm recordings corresponded to either point attractors (recordings 1–3) or limit cycles (recordings 4–9). This is in correspondence with the results reported in Hernandez et al. (1995a, b). Examples of E-NFR trajectories are shown in Fig. 6 (dashed lines).

5.3 Estimation of neural mass model parameters

The neural mass model was fitted to each recording using the nonlinear Kalman filter and ML estimation procedure described above. The parameters estimated for each recording and the likelihood of the model are shown in Table 2. These parameter values are in the range reported by Zetterberg et al. (1978). The variance of the innovation was, in all cases, less than 1% of the total signal power. However, these criteria were not used as a conclusive measure of the degree to which the model described the actual data correctly.

Rather, the quality of the fit should be measured by the degree to which the estimated model reproduces empirically observed dynamics of each recording. For this purpose, a model-based simulation for each recording was obtained by integrating the state equation (20) with the corresponding estimated parameters. Figure 3 (right) shows examples of simulated data. On the left are the actual EEG recordings. In all cases, the simulations are similar to the real recordings.

A bootstrap confidence interval for the spectrum of each actual EEG data was calculated by fitting a linear auto-regressive model and generating time series by bootstrapping the residuals of the linear fit. Each spectrum estimated from the model-based simulation was then compared against the corresponding confidence interval. For all recordings except numbers 8 and 9, the model-based EEG spectra fell well within the confidence regions obtained from the real data. For these two recordings, the global shapes of the model-based spectra are similar to the real one. The difference seems to be a multiplication by a scale factor. This is illustrated in Fig. 4 for the recordings shown in Fig. 3.

The adequacy of the model was further examined by checking the innovation time series obtained by the use of the nonlinear Kalman filter. Examples of the innovation series are shown in Fig. 5 (left). On the right, the histogram of the innovation series is shown together with the fitted Gaussian distribution. A Gaussian distribution of the innovation series was only rejected for recordings 8 and 9.

Table 2. Parameters estimated from the fit of the neural model to the EEG recordings

Recording	c_1	c_2	c_3	c_4	Π	a ($\times 10^{-4}$)	σ_p^2	$l(\mathbf{z};\boldsymbol{\theta})$ ($\times 10^3$)
1	9.99	1.91	52.52	10^{-6}	607	3.2	13.50	4.29
2	10.0	2.29	60.85	7.5	320	2.1	26.7	5.03
3	10.0	2.56	89.68	11.58	181	3.9	16.77	4.2
4	10.04	2.12	44.68	9.11	209	3.5	15.73	4.39
5	10.03	2.16	42.57	8.95	229	4.7	18.81	4.22
6	10.01	2.55	62.29	10.2	247	3.3	21.64	6.03
7	10.04	2.19	38.52	7.9	292	2.5	11.0	5.85
8	10.04	2.43	37.87	3.53	560	1.8	9.07	5.87
9	10.08	5.67	36.49	1.69	863	5.8	2.12	4.16

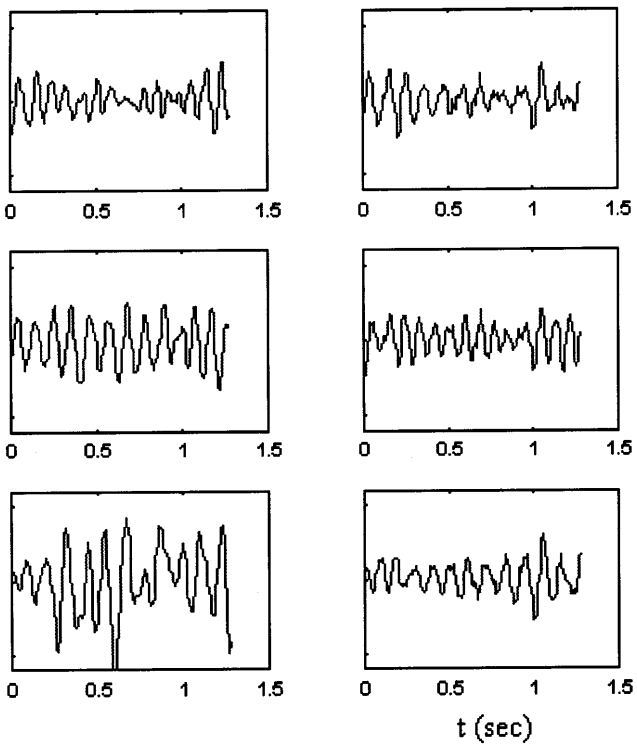

Fig. 3. *Left* Real EEG recordings 1, 5 and 9. *Right* Recordings simulated by integrating the state equation (20) using the estimated parameter values shown in Table 2

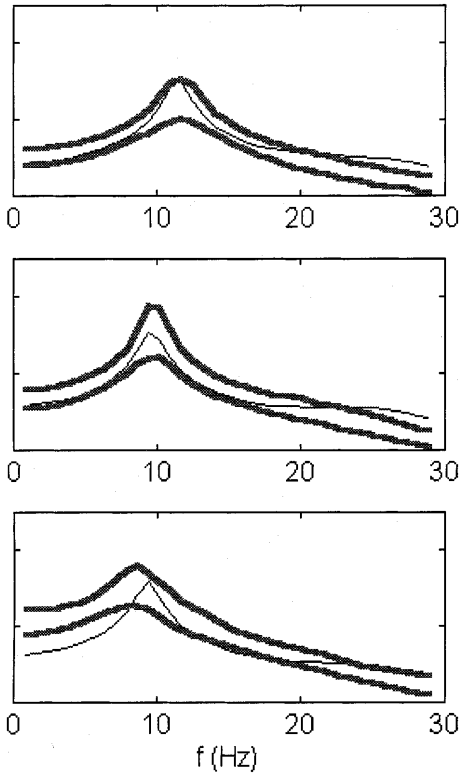

Fig. 4. Confidence interval (0.96) for the spectrum of the real data (*solid lines*) and spectrum estimated from model-based simulated EEG recording (*thin line*) shown in Fig. 3. *Top* Recordings 1, *middle* recording 5, and *bottom* recording 9

5.4 Neural mass model dynamics

Hopf bifurcations have been described for the noise-free neural mass model (Zetterberg et al. 1978). The existence of these bifurcations in brain dynamics has been empirically supported by the appearance of either limit cycles or point attractors in the E-NFR. In order to check whether the neural mass model can explain the dynamics of individual EEG time series, the following procedure was followed. Model NFRs (M-NFR) were obtained by the numerical integration of the ordinary differential equation (ODE) resulting from setting $\sigma^2 = 0$ in the state Eq. (20). The rest of the parameters were taken from Table 2. Then, the dynamics of the M-NFRs were compared with that of the E-NFRs. For the recordings 1–7, the qualitative behaviors of the E-NFR and M-NFR were similar. For the recordings 8 and 9, the E-NFR was a limit cycle and the M-NFR was a point attractor. Figure 6 shows examples of E-NFR and M-NFR for three recordings.

Though a complete analysis of the bifurcation behavior of the neural mass model is a formidable task, a preliminary exploration was undertaken. Changes in the behavior of the noise-free model fitted to each recording were evaluated by changing only parameter c_3. It was found that for some values of c_3 a Hopf bifurcation occurs. Moreover, it was found that a Hopf bifurcation occurs for some values of the parameter c_4, when the rest

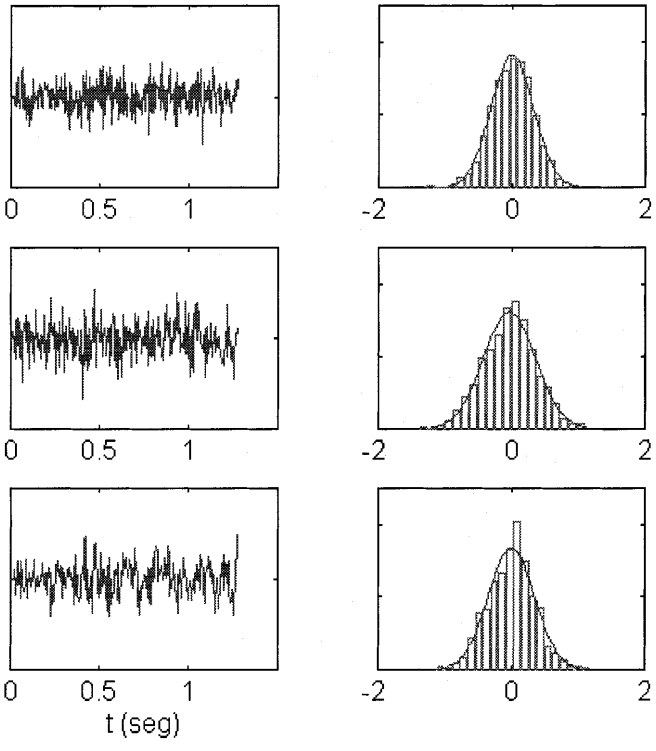

Fig. 5. *Left* Innovations obtained by local linearization filtering of the EEG recordings in Fig. 3 using, for each case, the estimated parameter values shown in Table 2 (recording 1, 5, 9). *Right* Histograms of innovations and estimated Gaussian distributions. The distribution of the innovation of recording 9 differs from the Gaussian at the 0.02 level (follows Kolmogorov-Smirnov test)

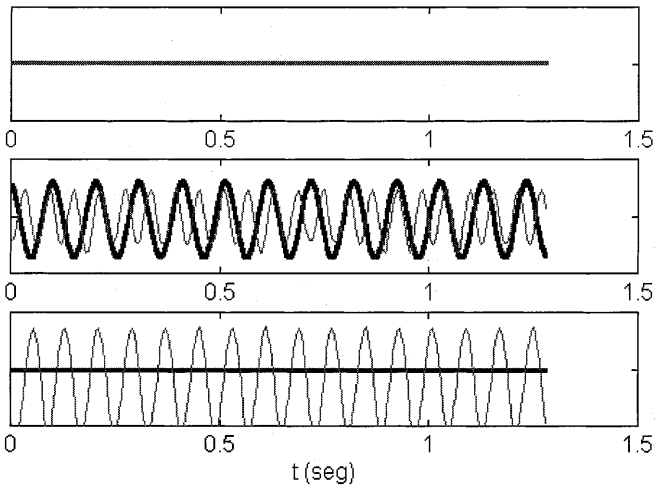

Fig. 6. Noise-free realizations corresponding to EEG recordings 1, 5, and 9. *Solid line* Simulation obtained by the numerical integration of the differential equation resulting in set $\sigma^2 = 0$ in the neural mass model and fixing the rest of the parameters with the values shown in Table 2 (model noise-free realization). *Thin line* Simulation obtained by suppressing noise in the nonparametric kernel auto-regressive estimator of each recording (empirical noise-free realization)

Table 3. Hopf bifurcation points. *Bifurcation point that could not be clearly identified

Recording	c_3	c_4
1	83	2.9
2	*	*
3	*	*
4	25.9	7.41
5	25.7	7.05
6	25.3	7.9
7	22.03	6.17
8	37.89	3.7
9	81	1.79

of the estimated parameters are left fixed. In Table 3 are shown the values of the parameters c_3 and c_4 for which Hopf bifurcation occurs. It should be noted that the estimated model parameters in Table 2 for recordings 8 and 9 are near the bifurcation parameters described in Table 3.

6 Discussion

This paper presents, to our knowledge, the first attempt to fit a continuous-time neural model to EEG data. The general statistical procedure described here allows the conversion of any neural mass models into nonlinear time series descriptions that can be directly fitted to the data. Moreover, since the estimation technique is based on the likelihood, the addition of penalty terms for model complexity (such as present in AIC, BIC, MLD, etc.) would allow the statistical comparison of different models.

Specifically, the neural mass model analyzed in this work is that proposed by Zetterberg et al. (1978) for the generation of alpha rhythms. This model is reformulated in the state space formalism and fitted to a set of alpha-rhythm recordings by means of the LL method. For all recordings, the variance of the residuals of the fitted model was less than 1% of the total signal power. In seven recordings, the residuals have a Gaussian distribution and the spectrum of the signal generated by the estimated model is not statistically different from that of the actual recording. Such a good fit is not achieved in only two recordings. This may be due to the fact that time delays are not included in the model, which modulate the shape of the spectral peak of the simulated EEG and may provide the extra flexibility necessary for fitting these recordings.

A relevant finding is the concordance of the dynamic behavior of the estimated model for each recording with that deduced by means of an empirical analysis of the EEG data. Nonparametric kernel estimates of alpha activity (Hernandez et al. 1995b) have shown that the alpha rhythm was heterogeneous with respect to its dynamic behavior. In many instances, alpha activity could be modeled as the output of linearly filtered white noise. In other cases, tests for linear behavior were clearly rejected. Nonparametric estimates of the attractors of these recordings were either point sets or limit cycles with no intermediate cases. We interpreted this as a type of "empirical bifurcation". This dichotomy was also found for the set of recordings analyzed in the present paper. A possible explanation for this observation is the Hopf bifurcation described by Zetterberg et al. (1978) for their model. Evidence for this hypothesis is provided by the correspondence between empirical and model noise-free realizations in all recordings for which there was a good fit.

Nevertheless, it is pertinent to remark that the Zetterberg model is only one of the simplest of continuous-time neural mass models. It is well known that this class of "lumped" models does not take into consideration important aspects of physiology and anatomy, i.e., the spatial distribution of neural masses (Van Rotterdam et al. 1982), intrinsic properties of neurons mediated by nonclassical ion currents (Wang 1994), etc. The relevance of the results is that such a simple model does indeed provide insight into some empirically observed nonlinear properties.

A number of prospective models (e.g., Nunez 1989; Wright et al. 1994; Zhadin 1994; Jirsa and Haken 1996; Robinson et al. 1997) for the alpha rhythms are currently available which differ in regard to physiological assumptions and computational complexity. Of special interest are the newer classes of models that extend the earlier neural mass models to consider spatially extended sets of neurons, thus involving partial differential equations (e.g., Jirsa and Haken 1996; Robinson et al. 1997). It will certainly be of interest to compare them with respect to their capability to predict EEG dynamic properties. For this purpose, the LL methodology used in this paper should be extended to the case of an evolution equation, a subject of current research.

Finally, it is to be hoped that the results presented here might be of some use in addressing the issue of

stochastic dynamics versus chaos in the nervous system. In recent years, there has been a tendency to view the EEG as the output of a low dimensional dynamic system with chaotic behavior (Elbert et al. 1994). An extreme point of view even banishes stochastic effects as an explanation for the EEG. The availability of parametric nonlinear models may be of assistance in assessing the role of stochastic effects in the EEG as well as to characterize the multiple dynamical attractors of the nervous system, some of which may or not be chaotic (cf. Achermann et al. 1994; Hernandez et al. 1996; Palus 1996; Valdes 1999). In the specific case of alpha rhythm, Soong and Stuart (1989) described the presence of chaotic dynamics. Our findings obtained by both empirically observed and model-derived dynamics are in disagreement with this observation.

However, the preferred model would be the one able to predict some real EEG property not trivially explicit in its formulation.

Acknowledgements. The authors thank F.H. Lopes da Silva and J.P. Pijn for their valuable suggestions and help. L.M. Rodriguez and J.L Hernadez gave essential aid in programming and testing, respectively, the methods described. Additionally, we would like to acknowledge the financial support by the Third World Academy of Sciences (TWAS) and the Ministry of Education, Science and Culture of Japan for exchange visits by Prof. T. Ozaki and J.C. Jimenez, respectively. The authors are also grateful to TWAS for the partial support of this work provided by Research Grant Project no. 96-206 RG/MATHS/LA and, also, to Takahashi Science Foundation.

References

Achermann P, Hartmann R, Gunzinger A, Guggenbühl W, Borbély A (1994) All-night sleep EEG and artificial stochastic control signals have similar correlation dimension. Electroenceph Clin Neurophysiol 90:384–387

Auestad B, Tjostheim D (1990) Identification of nonlinear time series: first order characterization and order determination. Biometrika 77:669–688

Biscay R, Jimenez JC, Riera J, Valdes P (1996) Local linearization method for the numerical solution of stochastic differential equations. Ann Inst Statist Math 48:631–644

Borisyuk RM, Kirilov AB (1992) Bifurcation analysis of a neural network model. Biol Cybern 66:319–325

Elbert T, Ray WJ, Kowalik AJ, Skinner JE, Graf KE, Birbaumer N (1994) Deterministic chaos in excitable cell assemblies. Physiol Rev 74:1–47

Freeman WJ (1975) Mass action in the nervous system. Academic Press, New York

Fundora A, Soler J, Tejeda J (1997) TrackWorker IV: user manual. Neuronic, SA, La Habana

Gumowski (1981) Qualitative properties of some dynamic systems with pure delay. In: Chevalet C, Micali A (eds) Lecture notes in biomathematics. Springer, New York Berlin Heidelberg

Hernandez JL, Valdes JL, Biscay R, Jimenez JC, Valdes P (1995a) EEG predictibility: properness of nonlinear forecasting methods. Int J Biomed Comput 38:197–206

Hernandez JL, Biscay R, Jimenez JC, Valdes PA, Grave de Peralta R (1995b) Measuring the dissimilarity between EEG recordings through a nonlinear dynamical system approach. Int J Biomed Comput 38:121–129

Hernandez JL, Valdes PA, Biscay R, Virues T, Szava S, Bosch J, Riquenes A, Clark I (1995c) A global scale factor in brain topography. Int J Neurosci 76:267–278

Hernandez JL, Valdes PA, Vila P (1996) EEG spike and wave modelled by a stochastic limit cycle. NeuroReport 7:2246–2250

Jimenez JC (1996) Local linealization method for the numerical solution of stochastic differential equations and nonlinear Kalman filters. In: Proc Symp: Studies on data analysis by statistical software, Fuji Kenshu-Jyo, Japan, Nov 1995, pp 291–292

Jimenez JC, Valdes PA, Rodriguez LM, Riera J, Biscay R (1998) Computing the noise covariance matrix of the local linealization scheme for the numerical solution of SDEs. Appl Math Lett 11:19–23

Jirsa VK, Haken (1996) A field theory of electromagnetic brain activity. Phys Rev Lett 77:960–963

Kaczmarek LK, Babloyantz A (1977) Spatio temporal patterns in epileptic seizures. Biol Cybern 26:199–208

Lopes da Silva FH, Hoeks A, Zetterberg LH (1974) Model of brain rhythmic activity, the alpha-rhythm of the thalamus. Kybernetik 15:27–37

Lopes da Silva FH, van Rotterdam A, Barts P, van Heusden E, Burr W (1976) Models of neuronal populations: the basic mechanisms. In: Corner MA, Swaab DF (eds) Perspectives of brain research. Prog Brain Res 45:281–308

Lopes da Silva FH (1993) Dynamics of EEG as signals of neuronal populations: models and theoretical considerations. In: Niedermeyer E, Lopes da Silva FH (eds) Electroencephalography: basic principles, clinical applications and related fields, 3rd edn. Williams and Wilkins, Baltimore-Munich

Nunez PL (1989) Generation of human EEG by a combination of long and short range neocortical interactions. Brain Topogr 1:198–215

Ozaki T (1985) Nonlinear time series models and dynamical systems. In: Hannan EJ, Krishnaiah PR, Rao MM (eds) Handb statistics 5:25–83

Ozaki T (1992) A bridge between nonlinear time series models and nonlinear stochastic dynamical systems: a local linearization approach. Stat Sin 2:113–135

Ozaki T (1993) A local linearization approach to nonlinear filtering. Int J Control 57:75–96

Ozaki T (1994) The local linearization filter with application to nonlinear system identifications. In: Bozdogan H (ed) Proceedings of the first US/Japan conference on the frontiers of statistical modeling: an informational approach. Kluwer Academic, Dordrecht, pp 217–240

Ozaki T, Jimenez JC, Haggan-Ozaki V (1996) Role of the likelihood function in the estimation of chaos models. Tech Rep 1996/11, University of Manchester, England

Palus M (1996) Nonlinearity in normal human EEG-Cycles, Temporal Asymmetry, Nonstationarity and Randomness, Not Chaos. Biol Cybern 75:389–396

Priestley MB (1988) Non-linear and non-stationary time series analysis. Academic Press, London

Robinson PA, Rennie CJ, Wright JJ (1997) Propagation and stability of wave of electrical activity in the cerebral cortex. Phys Rev E 56:826–840

Soong AC, Stuart CI (1989) Evidence of chaotic dynamics underlaying the human alpha-rhythm electroencephalogram. Biol Cybern 62:52–62

Szava S, Valdes P, Biscay R, Galan L, Bosch J, Clark I, Jimenez JC (1994) High resolution quantitative EEG analysis. Brain Top 6:211–219

Tong H (1990) Non-linear time series: a dynamical system approach. Clarendon Press, Oxford

Valdes PA, Bosch J, Jimenez JC, Trujillo N, Morales F, Biscay R, Hernandez JL, Ozaki T (1999) The statistical identification of nonlinear brain dynamics: a progress report. In: Pradhan N, Rapp PE, Sreenivasan (eds) Nonlinear dynamics and brain functioning Nova Science Publishers, Commack, NY

Van Rotterdam A, Lopes da Silva FH, Van der Ende J, Viergever MA, Hermans AJ (1982) A model of the spatio-temporal characteristics of the alpha rhythm. Bull Math Biol 44:283–305

Wang XJ (1994) Multiple dynamical modes of thalamic relay neurons: rythmic bursting and intermittent phase-locking. Neuroscience 59:21–31

Wiener N (1958) Nonlinear problems in random theory. MIT Press, Cambridge, Mass

Wilson HR, Cowan JD (1972) Excitatory and inhibitory interactions in localized populations of model neurons. Biophys J 12:2–24

Wright JJ, Sergejew AA, Liley DTJ (1994) Computer simulation of electrocortical activity at millimetric scale. Electroenceph Clin Neurophysiol 90:365–375

Zhadim MN (1994) Formation of rhythm processes in the bioelectric of the cerebral cortex. Biophysics 39:133–150

Zetterberg LH, Kristiansson L, Mossberg K (1978) Performance of a model for a local neural population. Biol Cybern 31:15–26